A Generalized Delayed Signal Cancellation Method for Detecting Fundamental-Frequency Positive-Sequence Three-Phase Signals

Francisco A. S. Neves, *Member, IEEE*, Marcelo Cabral Cavalcanti, *Member, IEEE*, Helber Elias Paz de Souza, Fabrício Bradaschia, Emilio J. Bueno, *Member, IEEE*, and Mario Rizo

***Abstract*—A novel scheme for obtaining the fundamental-frequency positive-sequence grid voltage vector based on a generalization of the delayed signal cancellation method is proposed in this paper. The technique is implemented by sampling and storing the instantaneous $\alpha\beta$ voltage vector. A mathematical transformation is then proposed through which the current and delayed voltage vectors are combined. It is shown that the proposed transformation has unity gain for the fundamental-frequency positive-sequence voltage vector, while its gain is equal to zero for some chosen components. Cascaded transformations can then be used for eliminating the fundamental-frequency negative-sequence vector, as well as chosen positive- and negative-sequence harmonic vector components and, thus, for accurately obtaining the fundamental-frequency positive-sequence voltage vector. The output of the last transformation block is input to a synchronous reference frame phase-locked loop for detecting frequency and position of the positive-sequence vector. A proposal for making the scheme frequency adaptive is also presented. The good performance of the proposed method is verified with simulations and experiments by using distorted and unbalanced signals, containing fundamental-frequency as well as positive- and negative-sequence harmonic components. The proposed method frequency adaptation capability is also verified.**

***Index Terms*—Converters, power quality (PQ), voltage control.**

I. Introduction

THE CORRECT value of the fundamental-frequency positive-sequence (FFPS) grid voltage vector is essential for achieving good control performance in grid-connected systems. Among the many applications of FFPS detection algorithms are series and shunt active filters, uninterruptible power supplies, adjustable speed drives, and renewable energy generation systems connected to the grid through voltage-source converters (VSC). This information is usually obtained by using a phase-locked loop (PLL). The PLL must be capable of following the FFPS voltage vector as fast as possible for eliminating the impacts of the grid signal imperfections [1]–[3].

The synchronous reference frame PLL (SRF-PLL) is frequently used in three-phase systems [2] and for balanced undistorted grid conditions, good results can be reached [4]. The SRF-PLL can also operate correctly if only high-order harmonics are present in the grid voltages, by reducing its bandwidth to attenuate these harmonics [5]. However, under unbalanced conditions, the second harmonic content of the voltage vector, caused by the negative-sequence components, makes the reduction of the bandwidth an inefficient solution, since the dynamics of the PLL would become very slow for such a narrow bandwidth. Better performance under unbalanced conditions can be achieved by separating the positive- and negative-sequence components of the voltage vector. This is made by the double synchronous reference frame PLL (DSRF-PLL) that uses a decoupling cell to isolate the positive- and negative-sequence fundamental-frequency components [6]. A cell for obtaining any other harmonic component may be implemented and then that component may be subtracted from the original voltages. However, the computational cost greatly increases if many harmonic components should be attenuated.

An alternative technique uses an enhanced PLL (EPLL) [7] for each phase. The phase voltages and their respective values delayed by 90° are used for obtaining the positive-sequence voltages of the three-phase system using the instantaneous symmetrical components (ISC) method [8], [9]. Finally, a fourth EPLL is applied to the output of the ISC method to estimate the positive-sequence voltage phase angle. The fundamental-frequency negative-sequence components of the grid voltages are eliminated by the EPLL calculator. However, some harmonics will pass through the EPLL and may be present in its output. In [8], an improved version of the method presented in [7] is obtained by omitting the fourth EPLL and combining the other three. Using this structure, a scheme for removing selected harmonic components is proposed in [10] at the expense of increase in complexity.

In the so-called delayed signal cancelation (DSC) method [11]–[14], the positive- and negative-sequence components of the grid voltage are separated based on the voltage vector in a stationary $(\alpha\beta)$ reference frame and on the voltage vector delayed by a quarter of cycle. After separation, the obtained positive-sequence α and β components are input to an SRF-PLL to calculate its amplitude and angular position. The method is suitable for unbalanced undistorted grid voltages, but the calcu-

Manuscript received June 22, 2009; revised September 11, 2009 and November 27, 2009. First published April 05, 2010; current version published June 23, 2010. Paper no. TPWRD-00463-2009.

F. A. S. Neves, M. C. Cavalcanti, and F. Bradaschia are with the Department of Electrical Engineering and Power Systems, Federal University of Pernambuco, Recife 50740-530, Brazil (e-mail: fneves@ufpe.br; marcelo.cavalcanti@ufpe.br; fabricionet@yahoo.com.br).

H. E. P. de Souza is with the Department of Industry, Federal Institute of Education, Pesqueira 55200-000, Brazil (e-mail: helberelias@yahoo.com.br).

E. J. Bueno and M. Rizo are with the Department of Electronics, University of Alcala, Madrid 28870, Spain (e-mail: emilio@depeca.uah.es; mario.rizo@depeca.uah.es).

Digital Object Identifier 10.1109/TPWRD.2010.2044196

lated positive- and negative-sequence voltages are sensitive to harmonics in the grid voltages.

Some other authors proposed different ways to combine resonant filters in order to prefilter the α and β input signals for determining the positive-sequence vector components. These components are then used in an output SRF-PLL for obtaining the positive-sequence vector amplitude and position [15]–[18]. In the so-called dual second-order generalized integrator-quadrature signal generator (DSOGI-QSG), the resonant filter parameters depend on the frequency detected by an output SRF-PLL in order to achieve a frequency-adaptive strategy. However, the robustness and stability to frequency variation have not yet been analyzed due to difficulties introduced by the nonlinearities involved. A frequency-locked loop (FLL) was proposed in [19] for substituting the output SRF-PLL of the DSOGI-QSG. In this case, the stability for small frequency deviations was demonstrated.

Usually, the discrete Kalman filter (DKF) is applied only in single-phase power systems [20]. Recent works propose the use of DKF for detecting the fundamental-frequency positive-sequence voltage vector in three-phase systems [21]–[23]. The KF gains are adjusted for rejecting the effects of low-order harmonics or negative-sequence components, but the response is slow compared to the previously mentioned techniques.

The Fourier transform has been used for many years for separating fundamental and harmonic components in single-phase signals. However, for three-phase signals, there is not an algorithm based on the Fourier transform to directly determine the FFPS and/or harmonic component vectors.

A frequency-domain detection method for sequence extraction from a three-phase signal was proposed in [24]. The method is based on different ways of applying the *Fortescue* transformation for obtaining the positive- and negative-sequence components of the grid voltage in order to eliminate specific harmonics from the original signals. The signal is passed through some cascaded mathematical transformations in order to cancel odd harmonics. However, the even harmonic components are not eliminated, although some of them may be attenuated.

Four mathematical transformations were used in [25] for eliminating odd and even harmonics. Two of these transformations are made in the stationary $\alpha\beta$ reference frame and they are able to remove odd harmonics from the original signals. The other two transformations are implemented in a synchronous dq reference frame, in order to cancel even harmonic components. This coordinate transformation requires the angular position of the FFPS vector, which is obtained from an output SRF-PLL. Demonstrating the stability of the angular position detection scheme in this case becomes a difficult nonlinear problem, since two mathematical transformation blocks are inside the output SRF-PLL control loop. As a consequence, the control parameters of the output SRF-PLL are difficult to be tuned for optimal performance and a frequency adaptation scheme was not proposed. This technique is referred to in this paper as EDSC-PLL (extended DSC-PLL).

This paper presents an original scheme that employs only simple calculations in the stationary $\alpha\beta$ reference frame and symmetrical components in the time domain [8] for extracting the FFPS grid voltages. The method is based on computing the instantaneous $\alpha\beta$ voltage vector and this vector delayed in time. A mathematical transformation is proposed through which the original and delayed voltage vectors are combined. It is shown that with the proposed generalized delayed signal cancelation (GDSC) technique, the transformation may be designed so that the FFPS voltage vector passes through it with unity gain. On the other hand, chosen positive- and negative-sequence harmonics components are eliminated. Cascaded transformations can then be used for accurately obtaining the FFPS voltage vector. The extracted FFPS is the input to an SRF-PLL for detecting frequency and position of the desired voltage vector. Any of these cascaded transformations is unconditionally stable and no transformation is inside the output SRF-PLL control loop.

This paper is organized as follows. The theoretical basis of the proposed GDSC technique is presented in Section II. This section also presents a way of cascading the proposed transformations for extracting the FFPS vector. A frequency adaptation scheme is then proposed. The performances of the GDSC method and other usual methods for obtaining the FFPS voltage vector are compared in Section III. The simulation cases were chosen based on the recommendations of usual standards and grid codes of some countries. Simulation and experimental results are shown in Section IV. Some implementation issues are also given. Conclusions are presented and discussed in Section V.

II. Proposed Method

A. Theoretical Generalization

Consider a three-phase set of unbalanced and distorted signals described by

$$\begin{cases} s_a = \sum_{h=0}^{\infty} \left[S_a^{(h)} \cos\left(h\omega t + \varphi_a^{(h)}\right) + S_0^{(h)} \cos\left(h\omega t + \varphi_0^{(h)}\right) \right] \\ s_b = \sum_{h=0}^{\infty} \left[S_b^{(h)} \cos\left(h\omega t + \varphi_b^{(h)}\right) + S_0^{(h)} \cos\left(h\omega t + \varphi_0^{(h)}\right) \right] \\ s_c = \sum_{h=0}^{\infty} \left[S_c^{(h)} \cos\left(h\omega t + \varphi_c^{(h)}\right) + S_0^{(h)} \cos\left(h\omega t + \varphi_0^{(h)}\right) \right]. \end{cases} \tag{1}$$

The hth harmonic component of the signals above can be written as follows:

$$\begin{cases} s_a^{(h)} = S_a^{(h)} \cos\left(h\omega t + \varphi_a^{(h)}\right) + S_0^{(h)} \cos\left(h\omega t + \varphi_0^{(h)}\right) \\ s_b^{(h)} = S_b^{(h)} \cos\left(h\omega t + \varphi_b^{(h)}\right) + S_0^{(h)} \cos\left(h\omega t + \varphi_0^{(h)}\right) \\ s_c^{(h)} = S_c^{(h)} \cos\left(h\omega t + \varphi_c^{(h)}\right) + S_0^{(h)} \cos\left(h\omega t + \varphi_0^{(h)}\right), \end{cases} \tag{2}$$

then

$$\begin{cases} s_a^{(h)} = S_a^{(h)} \frac{e^{j\left(h\omega t + \varphi_a^{(h)}\right)} + e^{-j\left(h\omega t + \varphi_a^{(h)}\right)}}{2} \\ \qquad + S_0^{(h)} \cos\left(h\omega t + \varphi_0^{(h)}\right) \\ s_b^{(h)} = S_b^{(h)} \frac{e^{j\left(h\omega t + \varphi_b^{(h)}\right)} + e^{-j\left(h\omega t + \varphi_b^{(h)}\right)}}{2} \\ \qquad + S_0^{(h)} \cos\left(h\omega t + \varphi_0^{(h)}\right) \\ s_c^{(h)} = S_c^{(h)} \frac{e^{j\left(h\omega t + \varphi_c^{(h)}\right)} + e^{-j\left(h\omega t + \varphi_c^{(h)}\right)}}{2} \\ \qquad + S_0^{(h)} \cos\left(h\omega t + \varphi_0^{(h)}\right). \end{cases} \tag{3}$$

These three-phase signals may be represented by a vector in a stationary $\alpha\beta$ reference frame, eliminating the effect of the homopolar components

$$\vec{s}_{\alpha\beta}^{(h)} = \frac{2}{3}\left(s_a^{(h)} + s_b^{(h)}e^{j2\pi/3} + s_c^{(h)}e^{-j2\pi/3}\right) \tag{4}$$

or

$$\vec{s}_{\alpha\beta}^{(h)} = e^{jh\omega t}\left[\frac{1}{3}\left(\tilde{S}_a^{(h)} + \tilde{S}_b^{(h)}e^{j2\pi/3} + \tilde{S}_c^{(h)}e^{-j2\pi/3}\right)\right] + e^{-jh\omega t}\left[\frac{1}{3}\left(\tilde{S}_a^{(h)} + \tilde{S}_b^{(h)}e^{-j2\pi/3} + \tilde{S}_c^{(h)}e^{j2\pi/3}\right)\right]^* \tag{5}$$

where the complex quantities indicated by the symbol $\tilde{S}$ are phasors, containing the information about the initial values of magnitude and phase angle of sinusoidal components

$$\tilde{S}_i^{(h)} = S_i^{(h)}e^{j\varphi_i^{(h)}}, \quad i = a, b, c. \tag{6}$$

It can also be observed from (5) that the terms inside the brackets are the Fortescue's positive- and negative-sequence phasors, denoted here by $\tilde{S}_{\alpha\beta+}^{(h)}$ and $\tilde{S}_{\alpha\beta-}^{(h)}$. Then

$$\vec{s}_{\alpha\beta}^{(h)} = \vec{s}_{\alpha\beta+}^{(h)} + \vec{s}_{\alpha\beta-}^{(h)} = \tilde{S}_{\alpha\beta+}^{(h)}e^{jh\omega t} + \tilde{S}_{\alpha\beta-}^{(h)*}e^{-jh\omega t}. \tag{7}$$

Without loss of generality, the positive- or the negative-sequence vector harmonic component can be represented by

$$\vec{s}_{\alpha\beta}^{(h_s)} = S_{\alpha\beta}^{(h_s)}e^{sign(h_s)j\varphi^{(h_s)}}e^{jh_s\omega t} \tag{8}$$

where

$$h_s = \begin{cases} h, & \text{for positive-sequence harmonic components} \\ -h, & \text{for negative-sequence harmonic components.} \end{cases} \tag{9}$$

Consider a positive- or negative-sequence vector harmonic component delayed in time by an angle corresponding to θ radians of the fundamental-frequency (or $h\theta$ radians with respect to the h_s harmonic component)

$$\vec{s}_{\alpha\beta-\theta}^{(h_s)} = S_{\alpha\beta}^{(h_s)}e^{sign(h_s)j\varphi^{(h_s)}}e^{jh_s(\omega t-\theta)} = \vec{s}_{\alpha\beta}^{(h_s)}e^{-jh_s\theta}. \tag{10}$$

It should be noted that if $h_s > 0$, then the voltage vectors $\vec{s}_{\alpha\beta}^{(h_s)}$ and $\vec{s}_{\alpha\beta-\theta}^{(h_s)}$ rotate counterclockwise and vector $\vec{s}_{\alpha\beta-\theta}^{(h_s)}$ is $h\theta$ radians behind $\vec{s}_{\alpha\beta}^{(h_s)}$. Conversely, if $h_s < 0$, then the voltage vectors $\vec{s}_{\alpha\beta}^{(h_s)}$ and $\vec{s}_{\alpha\beta-\theta}^{(h_s)}$ rotate clockwise and vector $\vec{s}_{\alpha\beta-\theta}^{(h_s)}$ is $h\theta$ radians in advance. In both cases, counterclockwise was considered to be the positive direction.

A mathematical transformation in which the original and delayed voltage vectors are combined is now proposed

$$\vec{s}_{\alpha\beta T}^{(h_s)} = \vec{a}\vec{s}_{\alpha\beta}^{(h_s)} + \vec{a}e^{j\theta_1}\vec{s}_{\alpha\beta-\theta}^{(h_s)} \tag{11}$$

where the complex gain $\vec{a}$ and the angle θ_1 are constants.

The aforementioned transformation allows choosing some specific harmonic components of the original signal to be eliminated. It is desirable, however, that the transformation gain for the FFPS voltage vector (or any other chosen harmonic component to be detected, with positive or negative sequence) could be made equal to one.

From (10) and (11), it can be easily verified that the transformed voltage vector $\vec{s}_{\alpha\beta T}^{(h_s)}$ is equal to the original signal $\vec{s}_{\alpha\beta}^{(h_s)}$ multiplied by complex gain

$$\vec{s}_{\alpha\beta T}^{(h_s)} = \underbrace{\vec{a}(1 + e^{j\theta_1}e^{-jh_s\theta})}_{\vec{G}^{(h_s)}} \times \left(S_{\alpha\beta}^{(h_s)}e^{sign(h_s)j\varphi^{(h_s)}}e^{jh_s\omega t}\right) \tag{12}$$

$$\vec{s}_{\alpha\beta T}^{(h_s)} = \vec{G}^{(h_s)}\vec{s}_{\alpha\beta}^{(h_s)}. \tag{13}$$

The real parameters θ and θ_1 are determined so that chosen harmonic components of order $h_s = h_i \pm kn$, $\forall n \in \mathbb{N}$, are eliminated, where h_i and k are chosen as constant integers. This is achieved by making $\vec{G}^{(h_i \pm kn)} = 0$

$$1 + e^{j\theta_1}e^{-j(h_i \pm kn)\theta} = 0 \Rightarrow \begin{cases} \theta = \frac{360^\circ}{k} \\ \theta_1 = \theta h_i + 180^\circ. \end{cases} \tag{14}$$

The complex constant parameter $\vec{a}$ is determined by imposing the desired transformation gain for a specific frequency vector. For example, in order to ensure unity gain for the FFPS voltage vector

$$\vec{G}^{(h_s=1)} = \vec{a}\left(1 + e^{j(\theta_1-\theta)}\right) = 1 \Rightarrow \vec{a} = \frac{1}{1 + e^{j(\theta_1-\theta)}}. \tag{15}$$

B. Implementation of the Proposed Method

An ideal FFPS voltage vector detector should be able to eliminate the fundamental-frequency negative-sequence vector along with all positive- and negative-sequence harmonic vectors. On the other hand, the gain for the FFPS vector should be equal to one. It is not possible to cancel all harmonic component vectors using only one transformation of the type described in (11). However, some transformations may be chosen to be put in cascade for eliminating harmonic component vectors around the FFPS vector.

As shown in (14), all even harmonic component vectors can be eliminated by a transformation in which $\theta = 180^\circ$ and $\theta_1 = 180^\circ$, where $\vec{a} = 1/2$ is chosen to keep the unitary gain for the FFPS voltage vector (15). Thus, the gain $\vec{G}_A^{(h_s)}$ for this first transformation is

$$\vec{G}_A^{(h_s)} = \frac{1}{2}\left[1 + e^{j180^\circ(1-h_s)}\right]. \tag{16}$$

Four other transformations (B, C, D, and E) were chosen in order to eliminate the harmonic vectors of order $h_s = 3 \pm 6n$, $h_s = 5 \pm 6n$, $h_s = 7 \pm 12n$, and $h_s = 13 \pm 24n$, respectively. The parameters for these transformations are $\theta_B = 60^\circ$, $\theta_{1B} = 0^\circ$, and $\vec{a}_B = (\sqrt{3}/3)e^{j30^\circ}$; $\theta_C = 60^\circ$, $\theta_{1C} = 120^\circ$ and $\vec{a}_C = (\sqrt{3}/3)e^{-j30^\circ}$; $\theta_D = 30^\circ$, $\theta_{1D} = 30^\circ$ and $\vec{a}_D = 1/2$; $\theta_E = 15^\circ$, $\theta_{1E} = 15^\circ$ and $\vec{a}_E = 1/2$. The corresponding gains are

$$\vec{G}_B^{(h_s)} = \frac{\sqrt{3}}{3}e^{j30^\circ}\left[1 + e^{-j60^\circ h_s}\right], \tag{17}$$

$$\vec{G}_C^{(h_s)} = \frac{\sqrt{3}}{3}e^{-j30^\circ}\left[1 + e^{j(2-h_s)60^\circ}\right], \tag{18}$$

$$\vec{G}_D^{(h_s)} = \frac{1}{2}\left[1 + e^{j(1-h_s)30^\circ}\right], \tag{19}$$

$$\vec{G}_E^{(h_s)} = \frac{1}{2}\left[1 + e^{j(1-h_s)15^\circ}\right]. \tag{20}$$

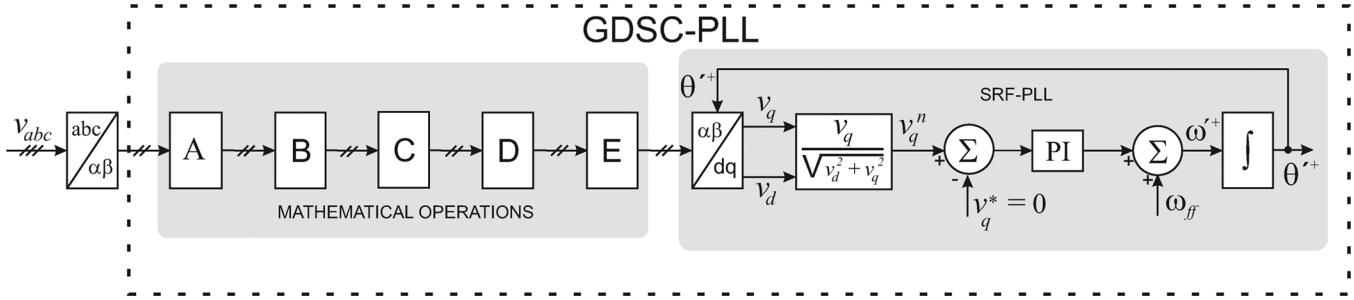

Fig. 1. Block diagram of the proposed solution without the frequency adaptation scheme.

In order to exemplify the proposed method, transformations A, B, C, D, and E are cascaded, as shown in Fig. 1. Using this proposed solution, only the positive- and negative-sequence harmonics of order $1 \pm 24n$ are not canceled by the mathematical operations. These harmonic components can be attenuated by adequately choosing the bandwidth of the output SRF-PLL. The decision about the bandwidth of the output PLL must take into consideration the increase in the overall response time of the FFPS vector detection scheme versus the total harmonic distortion (THD) reduction achieved.

The first step for implementing each transformation is measuring the phase quantities and calculating vector $\vec{s}_{\alpha\beta}$. The vector components must be stored in order to determine $\vec{s}_{\alpha\beta-\theta}$. The transformed vector is obtained by summing the current and the delayed vectors multiplied by $\vec{a}$ and $\vec{a}e^{j\theta_1}$, respectively. This is done in a matrix form by performing the following operation:

$$\begin{bmatrix} s_{\alpha T} \\ s_{\beta T} \end{bmatrix} = \begin{bmatrix} a_1 & -a_2 \\ a_2 & a_1 \end{bmatrix} \begin{bmatrix} s_\alpha \\ s_\beta \end{bmatrix} + \begin{bmatrix} b_1 & -b_2 \\ b_2 & b_1 \end{bmatrix} \begin{bmatrix} s_{\alpha-\theta} \\ s_{\beta-\theta} \end{bmatrix} \quad (21)$$

where $a_1 = real(\vec{a})$, $a_2 = imag(\vec{a})$, $b_1 = real(\vec{a}e^{j\theta_1})$, and $b_2 = imag(\vec{a}e^{j\theta_1})$.

Consequently, transformations A, B, C, D, and E are implemented through very low computational effort operations

$$\begin{bmatrix} s_{\alpha TA} \\ s_{\beta TA} \end{bmatrix} = \frac{1}{2} \begin{bmatrix} s_\alpha - s_{\alpha-180} \\ s_\beta - s_{\beta-180} \end{bmatrix}, \quad (22)$$

$$\begin{bmatrix} s_{\alpha TB} \\ s_{\beta TB} \end{bmatrix} = \frac{1}{2} \begin{bmatrix} 1 & -\frac{\sqrt{3}}{3} \\ \frac{\sqrt{3}}{3} & 1 \end{bmatrix} \begin{bmatrix} s_{\alpha TA} + s_{\alpha TA-60} \\ s_{\beta TA} + s_{\beta TA-60} \end{bmatrix}, \quad (23)$$

$$\begin{bmatrix} s_{\alpha TC} \\ s_{\beta TC} \end{bmatrix} = \frac{1}{2} \begin{bmatrix} 1 & \frac{\sqrt{3}}{3} \\ -\frac{\sqrt{3}}{3} & 1 \end{bmatrix} \begin{bmatrix} s_{\alpha TB} \\ s_{\beta TB} \end{bmatrix} + \begin{bmatrix} 0 & -\frac{\sqrt{3}}{3} \\ \frac{\sqrt{3}}{3} & 0 \end{bmatrix} \begin{bmatrix} s_{\alpha TB-60} \\ s_{\beta TB-60} \end{bmatrix}, \quad (24)$$

$$\begin{bmatrix} s_{\alpha TD} \\ s_{\beta TD} \end{bmatrix} = \frac{1}{2} \begin{bmatrix} s_{\alpha TC} \\ s_{\beta TC} \end{bmatrix} + \frac{1}{4} \begin{bmatrix} \sqrt{3} & -1 \\ 1 & \sqrt{3} \end{bmatrix} \begin{bmatrix} s_{\alpha TC-30} \\ s_{\beta TC-30} \end{bmatrix}, \quad (25)$$

$$\begin{bmatrix} s_{\alpha TE} \\ s_{\beta TE} \end{bmatrix} = \frac{1}{2} \begin{bmatrix} s_{\alpha TD} \\ s_{\beta TD} \end{bmatrix} + \frac{1}{2} \begin{bmatrix} \frac{\sqrt{2+\sqrt{3}}}{2} & -\frac{\sqrt{2-\sqrt{3}}}{2} \\ \frac{\sqrt{2-\sqrt{3}}}{2} & \frac{\sqrt{2+\sqrt{3}}}{2} \end{bmatrix} \begin{bmatrix} s_{\alpha TD-15} \\ s_{\beta TD-15} \end{bmatrix}. \quad (26)$$

It must be noted that the output PLL does not influence transformations $A - E$, since they are all implemented in $\alpha\beta$ (i.e., transformations $A - E$ do not use the angular position estimated by the output SRF-PLL), as occurred in the EDSC-PLL method [25]. The output SRF-PLL transfer function may be obtained by considering that the estimated output vector position (θ'^{+}) is approximately equal to the correct value (θ) [5]. The vector v_q obtained from the $\alpha\beta$ to dq transformation was normalized for making the PLL transfer function independent from the voltage vector magnitude. For achieving an overshoot of 20% independently from the bandwidth, the parameters were calculated by considering a relative damping factor $\xi = 1/\sqrt{2}$ [26]. However, the natural frequency choice depends on the lowest order harmonic component that must be filtered by the output PLL. The lower the natural frequency is, the lower the bandwidth of the PLL is and the slower its response will be. Using the SRF-PLL, a low natural frequency must be chosen in order to filter out the effects of low-order harmonics on the output voltage. For the proposed method, a much higher bandwidth may be specified, since most low-order harmonics are eliminated by the cascaded transformations.

As indicated in (11), the transformed output vector $\vec{s}_{\alpha\beta T}$ is calculated by using the input vector $\vec{s}_{\alpha\beta}$ and from this vector, delayed in time by a value corresponding to θ radians of the fundamental frequency signal. Thus, the samples of the α and β components of a transformation input vector must be stored by the time delay period. For this reason, when a transformation input vector changes, the correct filtering action is achieved only after the time necessary for the delayed input signal become affected. The maximum overall response time of transformations $A - E$ corresponds to 345° of the fundamental frequency cycle (i.e., 19.17 ms if the grid frequency is 50 Hz). However, it should be pointed out that the proposed transformations are finite-impulse-response (FIR) filters and, therefore, do not change the input signals frequency is equal to the rated value. Furthermore, as shown in (27) and (28), if the input signal's frequency is equal to the rated value ($h_1 = 1$, where h_1 is the ratio between the actual and rated grid frequencies), then there will be no error in the detected magnitude or phase angle. Therefore, the ability of the output PLL stage to synchronize with the input fundamental frequency and detect the correct angle is maintained. The response time of the fundamental-frequency positive-sequence vector detection is the sum of transformations delays with that of the output PLL. On the other hand, a much faster output SRF-PLL may be used, since it will not need to filter low-order harmonics.

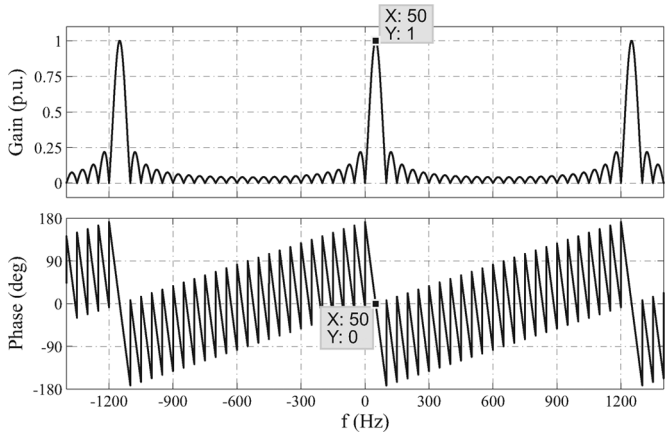

Fig. 2. Frequency response of the cascaded $A - E$ transformations.

C. Frequency Adaptation Scheme

If the grid frequency varies, the delays used in the proposed transformations will not correspond to 180°, 60°, 30°, or 15°. The detection algorithm takes 50 Hz as the fundamental frequency and the actual frequency will be filtered as an interharmonic component near the fundamental. In this case, the cascaded transformation gains and phase angles will be different than those for 50-Hz signals.

The transformations $A - E$ can be viewed as vector FIR filters applied to three-phase systems. An evaluation of the proposed transformations filtering performance can be made by computing the absolute value and phase angle of the cascaded gains given in (16)–(20) for different harmonic components, as shown in Fig. 2. In this figure, the negative frequency is used to indicate negative-sequence vector signals. Thus, in the described nonadaptive GDSC method, a fundamental frequency variation in the input signals causes magnitude and phase-angle errors in the positive-sequence detected vector. If transformations $A - E$ are used in cascade, then the per-unit magnitude error (ME_{pu}) and phase-angle error in degrees (PE_{deg}) can be obtained by

$$ME_{pu} = 1 - \left|\vec{G}_A^{(h_1)}\vec{G}_B^{(h_1)}\vec{G}_C^{(h_1)}\vec{G}_D^{(h_1)}\vec{G}_E^{(h_1)}\right|, \quad (27)$$

$$PE_{deg} = \frac{180}{\pi}\arg\left\{\vec{G}_A^{(h_1)}\vec{G}_B^{(h_1)}\vec{G}_C^{(h_1)}\vec{G}_D^{(h_1)}\vec{G}_E^{(h_1)}\right\}. \quad (28)$$

For example, the magnitude and phase-angle errors for a 10% increased input frequency are equal to 0.016 p.u. and $-17.2°$, respectively.

It can be easily verified from (28) that a frequency deviation causes a constant steady-state error in the angular position of the FFPS estimated vector (output from E). Thus, the E transformation output and the input signals have the same frequency. As a consequence, the frequency obtained from the output SRF-PLL is influenced only by components of frequency $(1 \pm 24n)f_1$, where $n \in \mathbb{N}$ and f_1 is the fundamental frequency. However, the components $\pm 24nf_1$ are strongly attenuated by the output SRF-PLL. The output frequency is then a very good estimate of the input signals' fundamental frequency.

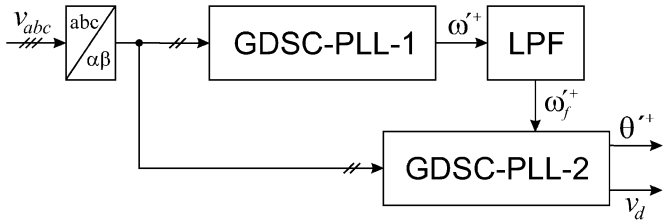

Fig. 3. Block diagram of the proposed solution with the frequency adaptation scheme.

The detected frequency can be used to determine the number of samples in one fundamental cycle and the number of samples corresponding to each delay in transformations $A - E$.

In order to reduce the GDSC mentioned errors due to frequency variations, a frequency-adaptive scheme using two GDSC-PLL blocks is proposed, as shown in Fig. 3. The GDSC-PLL-1 transformations $A - E$ use the rated grid frequency, but as discussed before, give the correct estimate of the actual system frequency. This estimated frequency is used to adapt the number of samples of GDSC-PLL-2 transformations $A - E$.

Using a constant sampling frequency, the number of samples corresponding to the delays in transformations $A - E$ should be adjusted when the input frequency varies, for keeping the transformation gains constant. However, the delay θ of a transformation may not correspond to an integer number of samples. The nearest integer is then used in the GDSC-PLL-2, causing an error in the transformation gain.

In order to compute the effect of the rounding error over operations $A - E$, let $N_\theta \in \mathbb{R}$ be the number of samples that correspond to the delay θ in (11) and $N_{d\theta} \in \mathbb{N}$ the integer number nearest to N_θ. Thus, the delayed signal actually used in the transformation is

$$\vec{s}_{\alpha\beta-\theta d}^{(h_s)} = \vec{s}_{\alpha\beta}^{(h_s)} e^{-jh_s\theta_d} \quad (29)$$

where $\theta_d = (N_{d\theta}/N)2\pi$.

The frequency-adaptive transformation gain becomes equal to

$$\vec{G}_{adapt}^{(h_s)} = \vec{a}(1 + e^{j\theta_1}e^{-jh_s\theta_d}). \quad (30)$$

Considering a fixed sampling frequency of 18 kHz and using (30), the magnitude and phase angle of the cascaded $A - E$ transformations were computed and plotted in Fig. 4. As can be observed for input signals frequency varying from 40 to 60 Hz, the maximum phase-angle error caused by rounding the delays to the nearest number of integer sampling periods is around one degree. The magnitude error is negligible.

A low-pass filter (LPF) is recommended because the GDSC-PLL-1 output frequency oscillates during the first milliseconds after a severe disturbance in the grid signals. Since the frequency in a power system does not experiment fast transients, an LPF with a low cutoff frequency should be used.

The computational burden for implementing transformations $A - E$ is very low (16 real multiplications and 18 real sums). For this reason, the use of two GDSC-PLL blocks for achieving

TABLE I
INDIVIDUAL HARMONIC VOLTAGE LIMITS IN LOW- AND MEDIUM-VOLTAGE NETWORKS (PERCENT OF FUNDAMENTAL COMPONENTS) [27], [28]

Odd harmonics non-multiple of 3		Odd harmonics multiple of 3		Even harmonics	
Order h	Voltage (%)	Order h	Voltage (%)	Order h	Voltage (%)
5	6	3	5	2	2
7	5	9	1.5	4	1
11	3.5	15	0.4	6	0.5
13	3	21	0.3	8	0.5
17 - 49	$v_1(h)$	21 - 45	0.2	10 - 50	$v_2(h)$

The corresponding compatibility level for the total harmonic distortion is $\mathrm{THD} = 8\%$.
$v_1(h) = (2.27(17/h) - 0.27)\%$ and $v_2(h) = (0.25(10/h) + 0.25)\%$.

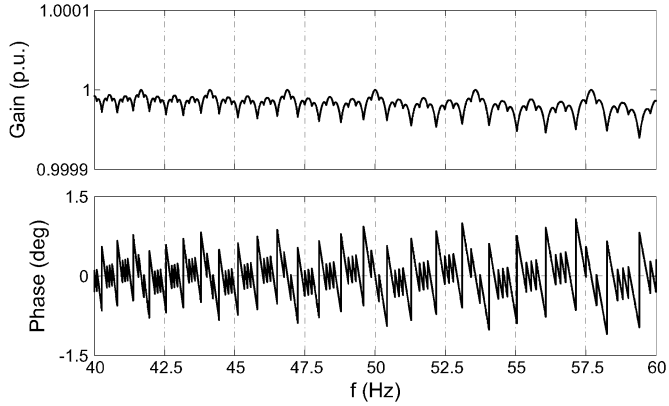

Fig. 4. Magnitude and phase angle of the detected FFPS signal by using the cascaded adaptive $A - E$ transformations.

a frequency-adaptive scheme can be executed in usual digital processors.

III. COMPARISON OF SYNCHRONIZATION METHODS

In order to verify the proposed algorithm effectiveness, simulations were carried out for obtaining the positive-sequence fundamental-frequency voltages from unbalanced and distorted input signals. The grid fundamental frequency is 50 Hz and the sampling frequency is 18 kHz. In all situations, the prefault voltage is $v_{pf}^{+1} = 1\angle 0^\circ$ p.u. After that, different disturbances are applied during 120 ms and then the initial balanced undistorted input voltages are restored. These simulation cases are used to compare the performance of the proposed technique with usual synchronization methods.

The grid codes of most countries require wind farms to remain connected to the grid during severe voltage sags. In some cases, restrictions are also demanded in terms of the renewable energy source ability to control the active and reactive power during and after the fault [27]. For attending these requirements, the fast detection of the FFPS voltage vector is very important. In the first simulation case, a three-phase balanced voltage sag with a phase jump of 20° is considered. During the fault, the remaining voltage is 15%. Further, 6% of 5th negative-sequence and 5% of 7th positive-sequence harmonic voltage vectors are added to the fundamental-frequency components.

The second and third tests consider the application of phase-to-neutral and phase-to-phase voltage sags, respectively. In both cases, the test recommendations of IEC 61000 standards for a system with a remaining voltage of 40% are followed [29]. The phase voltages in the phase-to-neutral voltage dip are equal to $0.4\angle 0^\circ$ p.u., $1.0\angle -120^\circ$ p.u., and $1.0\angle 120^\circ$ p.u., respectively. In the phase-to-phase case, these phase voltages are $0.53\angle -79^\circ$ p.u., $1.0\angle -120^\circ$ p.u., and $1.0\angle 120^\circ$ p.u., respectively. The same fifth and seventh harmonic voltage vector components of case 1 are considered during the fault.

In the fourth simulation case, highly distorted input signals are considered. The harmonic components of the three-phase test voltages are the maximum-allowed values according to IEC standards [27], [28] as indicated in Table I. These standards do not specify the angle of each harmonic component vector. In the simulations presented, each angle is equal to the respective harmonic order, in degrees.

According to some grid codes [27], wind turbines connected to the distribution system must remain connected during a rate of change in frequency up to and including 0.5 Hz/s. Another requirement is that a single-phase jump of 20° in the point of common coupling (PCC) should not initiate a regulation of the frequency, which occurs typically if the detected frequency goes outside the range $48.7\ \mathrm{Hz} \leq f \leq 51.3\ \mathrm{Hz}$. These frequency requirements are verified through two more simulation tests. In the fifth test, after the first second, a fundamental-frequency reduction of 0.5 Hz/s is simulated until the frequency reaches 47 Hz and after that, the frequency remains equal to 47 Hz. In the last test, a 20° phase jump in the FFPS voltage vector is considered in order to verify whether the detected frequency reaches the limit for initiating the frequency regulation scheme.

Table II provides a quantitative comparison of the proposed methods with five existing synchronization methods, based on the output total harmonic distortion (THD) and response time. The methods used for comparison are the SRF-PLL, DSRF-PLL, DSOGI-PLL, DKF, EDSC-PLL, and the proposed methods, without (GDSC-PLL) and with the frequency adaptation scheme (GDSC-A-PLL), as shown in Fig. 3.

The DKF method used in comparisons with the proposed method is the one presented in [22], where the DKF is modeled by using four state variables: the three positive-sequence phase components plus a fourth state for allowing the phase-angle detection without an external PLL. The average values of the process and measurement noises are assumed to be zero, with covariance matrices defined as

$$E\left[w_k w_k^T\right] = Q_k$$
$$E\left[v_k v_k^T\right] = R_k. \tag{31}$$

The measurement noise covariance R is a diagonal matrix obtained prior to the filter operation. The determination of the process noise covariance Q is generally more difficult because

TABLE II
COMPARISON OF THE SYNCHRONIZATION METHODS

	SRF [2]	DSRF [6]	DSOGI [17]	DKF [22]	EDSC [25]	GDSC	GDSC-A
THD(1)	0.46 %	5.59 %	5.46 %	0.56 %	0.00 %	0.00 %	0.00 %
THD(2)	3.70 %	1.13 %	1.12 %	0.10 %	0.00 %	0.00 %	0.00 %
THD(3)	6.33 %	1.24 %	1.31 %	0.12 %	0.00 %	0.00 %	0.14 %
THD(4)	1.88 %	2.22 %	2.17 %	0.24 %	0.08 %	0.14 %	0.14 %
THD(5)	0.00 %	0.00 %	0.00 %	0.00 %	1.83 %	0.00 %	0.00 %
THD(6)	0.00 %	0.00 %	0.00 %	0.00 %	1.83 %	0.00 %	0.00 %
response time(1)	162.8 ms	399.3 ms	151.7 ms	222.0 ms	52.0 ms	22.7 ms	22.7 ms
response time(2)	–	6.1 ms	7.6 ms	–	26.1 ms	17.3 ms	17.3 ms
response time(3)	–	54.6 ms	34.2 ms	–	32.9 ms	18.3 ms	18.3 ms
response time(4)	–	–	21.7 ms	0.0 ms	0.0 ms	0.0 ms	0.0 ms
response time(5)	25.4 ms	29.8 ms	28.3 ms	–	–	–	17.9 ms
response time(6)	26.2 ms	44.4 ms	28.2 ms	–	–	–	18.0 ms
offset compensation	NO	NO	NO	NO	YES	YES	YES
number of samples	–	–	–	–	840	690	1380

typically it is not possible to directly observe the estimated process. Therefore, it has been selected as a diagonal matrix, guaranteeing uncorrelated state variables, with a small value to assign a little uncertainty to the process model.

In Table II, the numbers inside parentheses indicate the case simulated as already described. For example, (1) means a three-phase balanced voltage sag with phase jump and fifth negative-sequence and seventh positive-sequence harmonics and (2) and (3) correspond to the described phase-to-neutral and phase-to-phase voltage sags, respectively, and so on. It is also shown in Table II whether the method is capable of compensating signals with dc offset.

The THD presented in Table II is the highest among those calculated for the three phases. In practice, the higher harmonic component of the THD that can be calculated is equal to half of the sample frequency of the input signals. In all simulations and experiments, the sample frequency is 18 kHz. Then, all THD results have harmonic components up to 9 kHz. For simulation cases 1 to 4, the THD was measured during the sixth cycle after the fault so that the positive-sequence detection method had already been stabilized. For the other cases, the THD was computed right after the frequency reaches its final value of 47 Hz. The THD was calculated from

$$THD = \sqrt{\frac{\sum_{h=2}^{\infty}\left(V'^{+}_{rms}(h)\right)^2}{V'^{+}_{rms}(1)^2}}100\% \tag{32}$$

where V'^{+}_{rms} is the rms value of the output voltage v'^{+}_a, v'^{+}_b or v'^{+}_c and h is each frequency component.

The response time in Table II is the time necessary for the detected angle absolute error to remain inside a tolerance range of 1.5° (0.0262 rad). In some cases, the detection method was not able to guarantee the error to remain in the tolerance range. In those cases, the response time was represented by "–." In (1), the detected angle error remained inside the tolerance range and the response time was indicated as 0.00 ms. In all situations, the proposed method led to zero steady-state error.

As can be seen, the performance of the proposed technique is better than any of the previous ones for the criteria considered in the comparison. The response delay in the proposed technique is caused mainly by the time necessary for obtaining the delayed signals for the cascaded GDSC transformations, since the output PLL and output filter may have a high bandwidth and, thus, a fast response. For each transformation $A-E$, the output values of v_α and v_β from the previous cascaded transformation must be stored in order to determine the delayed voltage vector. Thus, the total amount of real variables to be stored for the cascaded transformations is equal to twice the total number of samples necessary for the delays in the cascaded transformations. This number for EDSC-PLL and GDSC-PLL methods is also included in Table II.

IV. SIMULATION AND EXPERIMENTAL RESULTS

Experiments using a OMICRON-CMC256 programmable source [30] to generate the same simulated input voltages of cases (1) to (4) are presented. These signals were acquired using 12-b AD converters and processed in a floating point Texas TMS320C6713 DSP. A sampling rate of 18 kHz was chosen so that the number of samples corresponding to any of the delays in transformations $A-E$ is an integer [11]. In order to plot the output quantities, the DSP variables to be examined were sent to digital outputs and saved for plotting using MATLAB. Figs. 5–8 show the experimental results. Each one presents three graphics (from top to bottom): input phase voltages (v_{abc}), output phase voltages (v'^{+}_{abc}), and the angle of the FFPS voltage vector (θ'^{+}). The detected FFPS voltage vector magnitude is plotted together with the v'^{+}_{abc} voltages. In all cases, this amplitude becomes constant after approximately one fundamental period after the disturbance, which is in accordance with the simulation results. This constant amplitude indicates that the output signals become balanced three-phase signals. Further, the detected angle rate of change becomes constant. To recover correctly, the three-phase signal, the estimated v'^{+}_d, v'^{+}_q, and θ'^{+} are input to the inverse Park transformation.

Experimental results showing the error of the detected FFPS voltage vector position cannot be plotted since the actual position is not available. These errors obtained by simulations are presented in Fig. 9. The response times, close to one fundamental period, are in accordance with the theoretical predictions. However, a small remaining error is observed in the responses for cases (1) and (3), in which the system experiences a phase jump. This error is caused by the slow dynamics of the

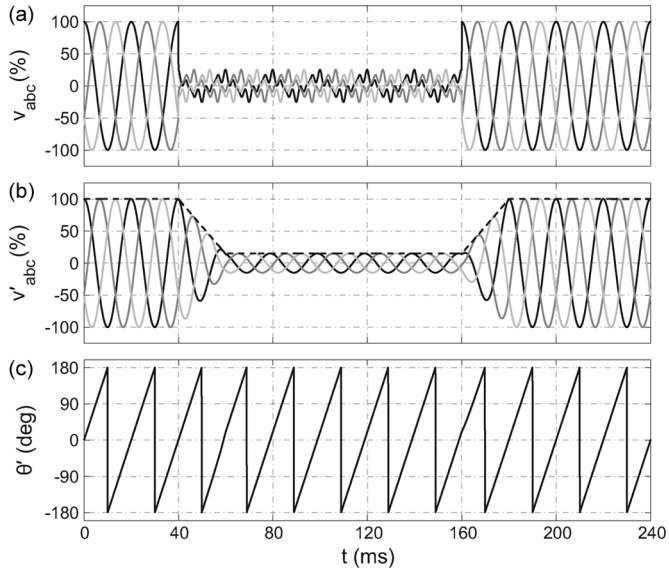

Fig. 5. Experimental results for case test (1). From top to bottom: the input voltages, the output voltages, and the FFPS angular position θ'^{+}.

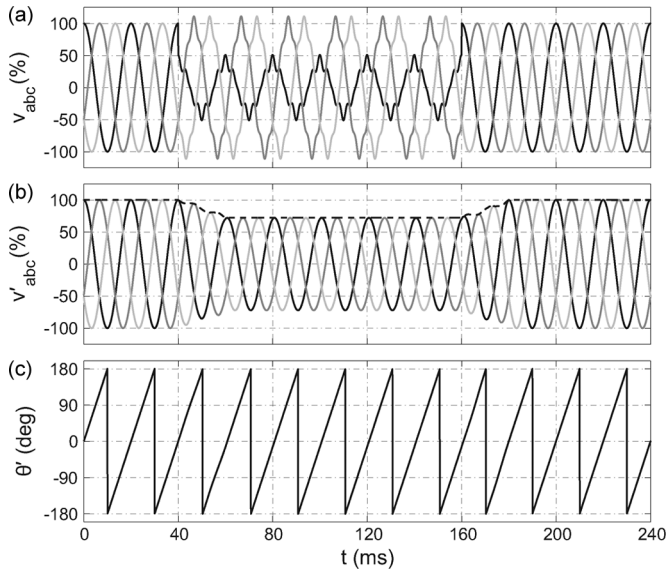

Fig. 6. Experimental results for case test (2). From top to bottom: the input voltages, the output voltages, and the FFPS angular position θ'^{+}.

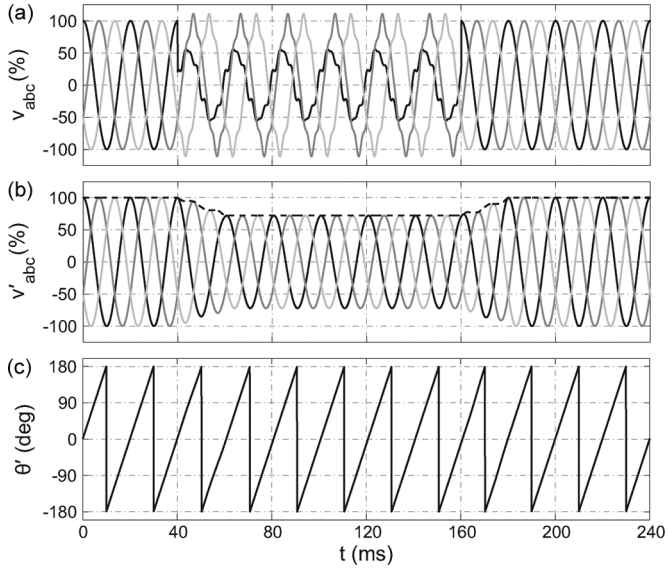

Fig. 7. Experimental results for case test (3). From top to bottom: the input voltages, the output voltages, and the FFPS angular position θ'^{+}.

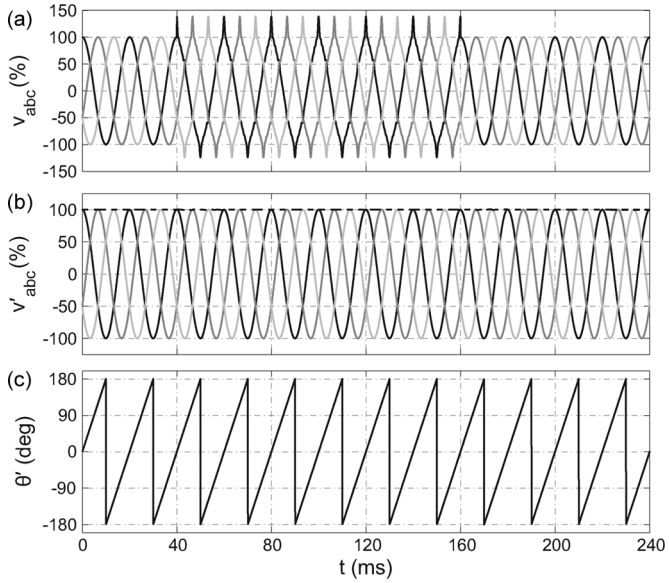

Fig. 8. Experimental results for case test (4). From top to bottom: the input voltages, the output voltages, and the FFPS angular position θ'^{+}.

detected frequency $\omega_f'^{+}$ (Fig. 3) and longer simulations showed that it converges to zero in approximately ten fundamental frequency periods.

V. Conclusion

In this paper, a method for obtaining the FFPS voltage vector in three-phase grid-connected systems is proposed and analyzed. The method is based on a generalized delayed signal cancelation process and uses only simple mathematical transformations in the stationary reference frame. It is proved that the current and delayed $\alpha\beta$ voltage vectors may be combined in a mathematical transformation in order to cancel specific harmonic positive- and negative-sequence voltage vectors from the original signal. Further, it is shown that cascading five of the proposed transformations makes it possible to cancel the fundamental-frequency negative-sequence components and all positive- and negative-sequence harmonic voltage vectors up to 24th order and the dc offsets. The last transformation output signals are input to a SRF-PLL for obtaining the synchronous d and q components, the fundamental frequency vector, and the position of the FFPS vector. Since the $\alpha\beta$ components input to the SRF-PLL do not have any low-order harmonic components, a high bandwidth PLL may be used. A way of combining two GDSC-PLL blocks for making the strategy frequency adaptive is also proposed. The presented method performance was verified through simulation and experimental tests according to IEC standards. The test cases include balanced and unbalanced voltage sags, harmonic distortion, and frequency variation. Compared to five other FFPS detection schemes, the proposed method presented the best performance in terms of detected

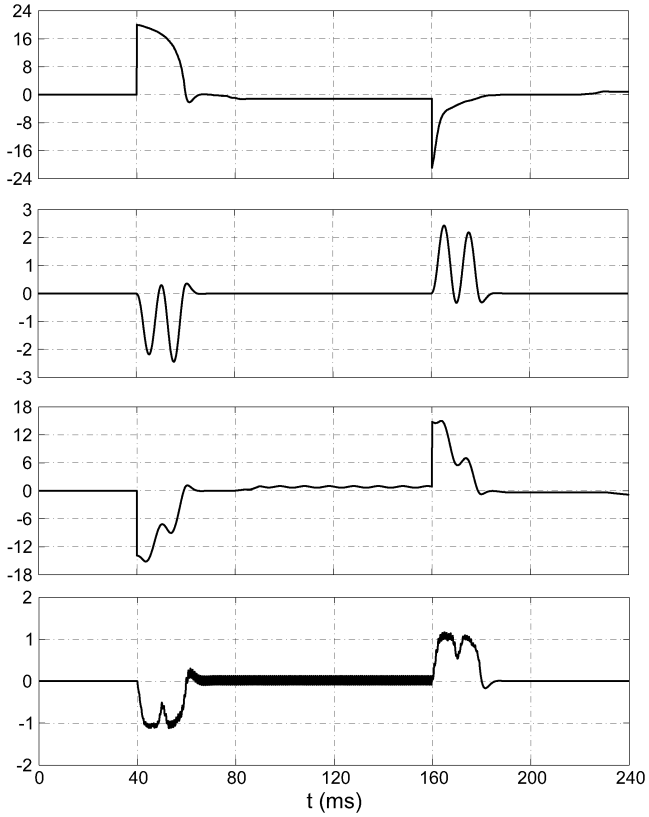

Fig. 9. Simulation results of the error in the detected FFPS voltage vector angular position for cases (1) to (4), respectively.

voltages THD and time response of the voltage vector-angle detection.

REFERENCES

[1] J. G. Nielsen, M. Newman, H. Nielsen, and F. Blaabjerg, "Control and testing of a Dynamic Voltage Restorer (DVR) at medium voltage level," *IEEE Trans. Power Electron.*, vol. 19, no. 3, pp. 806–813, May 2004.

[2] V. Kaura and V. Blasko, "Operation of phase locked loop system under distorted utility conditions," *IEEE Trans. Ind. Appl.*, vol. 33, no. 1, pp. 58–63, Jan./Feb. 1997.

[3] D. Yazdani, A. Bakhshai, G. Joos, and M. Mojiri, "A nonlinear adaptive synchronization technique for grid-connected distributed energy sources," *IEEE Trans. Power Electron.*, vol. 23, no. 4, pp. 2181–2186, Jul. 2008.

[4] L. N. Arruda, S. M. Silva, and B. J. C. Filho, "PLL structures for utility connected systems," in *Proc. Industry Applications Soc. Annu.Meet.*, Sep./Oct. 2001, vol. 4, pp. 2655–2660.

[5] S.-K. Chung, "A phase tracking system for three phase utility interfece inverters," *IEEE Trans. Power Electron.*, vol. 15, no. 3, pp. 431–438, May 2000.

[6] P. Rodríguez, J. Pou, J. Bergas, I. Candela, R. Burgos, and D. Boroyevich, "Decoupled double synchronous reference frame PLL for power converters control," *IEEE Trans. Power Electron.*, vol. 22, no. 2, pp. 584–592, Mar. 2007.

[7] M. Karimi-Ghartemani and M. R. Iravani, "A method for synchronization of power electronic converters in polluted and variable-frequency environment," *IEEE Trans. Power Syst.*, vol. 19, no. 3, pp. 1263–1270, Aug. 2004.

[8] M. Karimi-Ghartemani and H. Karimi, "Processing of symmetrical components in time-domain," *IEEE Trans. Power Syst.*, vol. 22, no. 2, pp. 572–579, May 2007.

[9] U. K. Rao, M. K. Mishra, and A. Ghosh, "Control strategies for load compensation using instantaneous symmetrical component theory under different supply voltages," *IEEE Trans. Power Del.*, vol. 23, no. 4, pp. 2310–2317, Oct. 2008.

[10] M. Karimi-Ghartemani, "A novel three-phase magnitude-phase-locked loop system," *IEEE Trans. Circuits Syst. I*, vol. 53, no. 8, pp. 1792–1802, Aug. 2006.

[11] J. Svensson, M. Bongiorno, and A. Sannino, "Practical implementation of delayed signal cancellation method for phase-sequence separation," *IEEE Trans. Power Del.*, vol. 22, no. 1, pp. 18–26, Jan. 2007.

[12] G. Saccomando and J. Svensson, "Transient operation of grid connected voltage source converter under unbalanced voltage conditions," in *Proc. IEEE Ind. Appl. Soc.*, 2001, pp. 2419–2424.

[13] M. Bongiorno, J. Svensson, and A. Sannino, "Effect of sampling frequency and harmonics on delay-based phase-sequence estimation method," *IEEE Trans. Power Del.*, vol. 23, no. 3, pp. 1664–1672, Jul. 2008.

[14] Z. Yao, "Fundamental phasor calcultion with short delay," *IEEE Trans. Power Del.*, vol. 23, no. 3, pp. 1280–1287, Jul. 2008.

[15] X. Yuan, W. Merk, H. Stemmler, and J. Allmeling, "Stationary-frame generalized integrators for current control of active power filters with zero steady-state error for current harmonics of concern under unbalanced and distorted operating conditions," *IEEE Trans. Ind. Appl.*, vol. 38, no. 2, pp. 523–532, Mar./Apr. 2002.

[16] R. I. Bojoi, G. Griva, V. Bostan, M. Guerriero, F. Farina, and F. Profumo, "Current control strategy for power conditioners using sinusoidal signal integrators in synchronous reference frame," *IEEE Trans. Power Electron.*, vol. 20, no. 6, pp. 1402–1412, Nov. 2005.

[17] P. Rodríguez, R. Teodorescu, I. Candela, A. Timbus, M. Liserre, and F. Blaabjerg, "New positive-sequence voltage detector for grid synchronization of power converters under faulty grid conditions," in *Proc. IEEE Power Electronics Specialists Conf.*, Jun. 2006, pp. 1–7.

[18] L. R. Limongi, R. I. Bojoi, C. Pica, F. Profumo, and A. Tenconi, "Analysis and comparison of phase locked loop techniques for grid utility applications," in *Proc. IEEE Power Conversion Conf.*, 2007, pp. 674–681.

[19] P. Rodríguez, A. Luna, I. Candela, R. Teodorescu, and F. Blaabjerg, "Grid synchronization of power converters using multiple second order generalized integrators," in *Proc. IEEE Annu. Conf. Industrial Electronics Soc.*, Nov. 2008, pp. 755–760.

[20] V. Moreno, M. Liserre, A. Pigazo, and A. Dell'Aquila, "A comparative analysis of real-time algorithms for power signal decomposition in multiple synchronous reference frames," *IEEE Trans. Power Electron.*, vol. 22, no. 4, pp. 1280–1289, Jul. 2007.

[21] A. Pigazo and V. Moreno, " $3\phi - 3w$ signal model for power system harmonics and unbalance identification using Kalman filtering," *IEEE Trans. Power Del.*, vol. 23, no. 2, pp. 1260–1261, Apr. 2008.

[22] M. S. Pádua, S. M. Deckmann, F. P. Marafão, and D. Colón, "Simplified models of Kalman filter for fundamental frequency, amplitude and phase angle detection," in *Proc. Brazilian Power Electronics Conf.*, Sep. 2007, pp. 175–180.

[23] M. S. Pádua, S. M. Deckmann, and F. P. Marafão, "Frequency-adjustable positive sequence detector for power conditioning applications," in *Proc. IEEE Power Electronics Specialists Conf.*, 2005, pp. 1928–1934.

[24] R. Cutri and L. Matakas, "A fast instantaneous method for sequence extraction," in *Proc. Brazilian Power Electronics Conf.*, Oct. 2007, pp. 1–6.

[25] H. E. P. de Souza, F. Bradaschia, F. A. S. Neves, M. C. Cavalcanti, G. M. S. Azevedo, and J. P. Arruda, "A method for extracting the fundamental frequency positive-sequence voltage vector based on simple mathematical transformations," *IEEE Trans. Ind. Electron.*, vol. 56, no. 5, pp. 1539–1547, May 2009.

[26] E. J. Bueno, F. J. Rodriguez, F. Espinosa, and S. Cobreces, "SPLL design to flux oriented of a VSC interface for wind power applications," in *Proc. IEEE Annu. Conf. Industrial Electronics Soc.*, Nov. 2005, pp. 1–6.

[27] F. Iov and F. Blaabjerg, "Advanced power converters for universal and flexible power management in future electricity network." Delivery D2.1 of UNIFLEX-PM. [Online]. Available: www.eee.nott.ac.uk/uniflex/Documents/W2-AU-DV-2001-B.pdf, Feb. 2007

[28] M. McGranaghan and G. Beaulieu, "Update on IEC 61000-3-6: Harmonic emission limits for customers connected to MV, HV and EHV," in *Proc. IEEE Transmission and Distribution Conf. Exhibit.*, May 2006, pp. 1158–1161.

[29] *Testing and measuring techniques—Voltage dips, short interruptions and voltage variations immunity tests for equipment with input current more than 16 A per phase*, IEC Std. 61000-4-34 Electromagnetic Compatibility (EMC) Part 4-34, 2004.

[30] Omicron CMC256—4 Phase Voltage/6 Phase Current Test Set. OMICRON–Testing solutions for protection and measurement systems., 2003.

Francisco A. S. Neves (M'00) was born in Campina Grande, Brazil, in 1963. He received the B.S. and M.Sc. degrees in electrical engineering from the Federal University of Pernambuco, Recife, Brazil, in 1984 and 1992, respectively, and the Ph.D. degree in electrical engineering from the Federal University of Minas Gerais, Belo Horizonte, Brazil, in 1999.

He was a Visiting Scholar at the Georgia Institute of Technology, Atlanta, in 1999, and at Alcala University, Spain, from 2008 to 2009. Since 1993, he has been with the Department of Electrical Engineering, Federal University of Pernambuco, where he is currently a Professor of Electrical Engineering. His research interests include power electronics, renewable energy systems, power quality, and grid synchronization methods.

Marcelo Cabral Cavalcanti (M'07) was born in Recife, Brazil, in 1972. He received the B.S. degree in electrical engineering from the Federal University of Pernambuco, Recife, Brazil, in 1997 and the M.S. and Ph.D. degrees in electrical engineering from the Federal University of Campina Grande, Campina Grande, Brazil, in 1999 and 2003, respectively.

Since 2003, he has been with the Department of Electrical Engineering, Federal University of Pernambuco, where he is currently a Professor of Electrical Engineering. His research interests are renewable systems, power quality, and three-phase matrix converters.

Helber Elias Paz de Souza was born in Cabo de Santo Agostinho, Brazil, in 1983. He received the B.S. and M.S. degrees in electrical engineering from the Federal University of Pernambuco, Recife, Brazil, in 2006 and 2008, respectively, where he is currently pursuing the Ph.D. degree.

Since 2009, he has been with the Department of Industry, Federal Institute for Education, Science and Technology of Pernambuco. His research interests are grid synchronization methods, power quality, and three-phase matrix converters.

Fabrício Bradaschia was born in São Paulo, Brazil, in 1983. He received the B.S. and the M.S. degrees in electrical engineering from the Federal University of Pernambuco, Recife, Brazil, in 2006 and 2008, respectively, where he is currently pursuing the Ph.D. degree.

From 2008 to 2009, he was a Visiting Scholar at the University of Alcalá, Madrid, Spain. His research interests are direct ac-ac converter topologies with high efficiency, pulsewidth modulation for three-phase matrix converters, discrete-time controls, and grid synchronization methods.

Emilio J. Bueno (S'05–M'06) was born in Madrid, Spain, in 1972. He received the M.S. and Ph.D. degrees in electronics engineering from the Universidad de Alcalá, Madrid, Spain, in 1999 and 2005, respectively.

Currently, he is an Associate Professor with the Department of Electronics, Universidad de Alcalá, where he is a member of the Research Group "Electronics Engineering Applied to the Renewable Energies." His research interests include power-electronic systems, control of power-electronic converters, power quality, and distributed power generation systems.

Mario Rizo received the M.D. degree in telecommunication engineering from the Alcalá University, Madrid, Spain, in 2009, where he is currently pursuing the Ph.D. degree.

Since 2007, he has been a member of the Electronic Engineering Applied to Renewable Energies Research Group of Alcalá University. His research areas include massive integration of renewable energies in power systems, control of power converters used in renewable energy systems, and power quality.